Computers, Materials & Continua CMC, vol.65, no.2, pp.1809-1823, 2020

Computational Analysis of the Effect of Nano Particle Material Motion on Mixed Convection Flow in the Presence of Heat Generation and Absorption

Muhammad Ashraf[1], Amir Abbas[1], Saqib Zia[2], Yu-Ming Chu[3, 4], Ilyas Khan[5, *] and Kottakkaran Sooppy Nisar[6]

Abstract: The present study is concerned with the physical behavior of the combined effect of nano particle material motion and heat generation/absorption due to the effect of different parameters involved in prescribed flow model. The formulation of the flow model is based on basic universal equations of conservation of momentum, energy and mass. The prescribed flow model is converted to non-dimensional form by using suitable scaling. The obtained transformed equations are solved numerically by using finite difference scheme. For the analysis of above said behavior the computed numerical data for fluid velocity, temperature profile, and mass concentration for several constraints that is mixed convection parameter λ_t, modified mixed convection parameter λ_c, Prandtl number Pr, heat generation/absorption parameter δ, Schmidt number Sc, thermophoresis parameter N_t, and thermophoretic coefficient k are sketched in graphical form. Numerical results for skin friction, heat transfer rate and the mass transfer rate are tabulated for various emerging physical parameters. It is reported that in enhancement in heat, generation boosts up the fluid temperature at some positions of the surface of the sphere. As heat absorption parameter is decreased temperature field increases at position $X = \pi/4$ on the other hand, no alteration at other considered circumferential positions is noticed.

Keywords: Nano material, mixed convection, finite difference method, heat generation/absorption, spheres.

[1] Department of Mathematics, Faculty of Science, University of Sargodha, Sargodha, 40100, Pakistan.

[2] Department of Mathematics, COMSATS University Islamabad, Islamabad, 44000, Pakistan.

[3] Department of Mathematics, Huzhou University, Huzhou, 313000, China.

[4] Hunan Provincial Key Laboratory of Mathematical Modeling and Analysis in Engineering, Changsha University of Science & Technology, Changsha, 410114, China.

[5] Faculty of Mathematics and Statistics, Ton Duc Thang University, Ho Chi Minh City, 72915, Vietnam.

[6] Department of Mathematics, College of Arts and Sciences, Prince Sattam bin Abdulaziz University, Wadi Aldawaser, 11991, Saudi Arabia.

[*] Corresponding Author: Ilyas Khan. Email: ilyaskhan@tdtu.edu.vn.

Received: 06 May 2020; Accepted: 22 May 2020.

1 Introduction

The phenomenon in which very small particles move away from the hot surface or come towards the cold surface due to the temperature gradient is known as thermophoretic motion or nano-particle material motion. Small particles such as dust particles when they are suspended in a gas that has a temperature gradient experience a force which is opposite to the direction of the temperature gradient, create what is called thermophoretic force. This phenomenon has diverse applications in nature and industry. In the current work, the main discussion is incorporated to the effect of nano-particle material motion and heat generation/absorption on mixed convection flow across the surface of a sphere. Abbas et al. [Abbas and Ashraf (2020)] examined numerically the combined effects of thermophoretic transportation and mixed convection flow with the inclusion of variable viscosity around a sphere. Ashraf et al. [Ashraf, Chamkha, Iqbal et al. (2016)] proposed the model of convective flow over a magnetized surface by taking the effect of variable viscosity and temperature-dependent thermal conductivity. The effect of viscous dissipation on periodic mixed convection flow around a sphere has been simulated numerically by Ashraf et al. [Ashraf, Fatima and Gorla (2017)]. Later, the solutions for time-dependent shear stress and heat transfer rate around various points of sphere associated with the fluid dissipation have been demonstrated by [Ashraf and Fatima (2018)]. Later, Ashraf et al. [Ashraf, Khan and Gorla (2019)] presented nano-fluid heat transfer through natural convection around a sphere and in the plume region developed above the sphere. Variable density effects on oscillatory mixed convection flow of an electrically conducting fluid along the non-conducting circular cylinder have been discussed by [Ashraf and Ullah (2020)]. Fagbade et al. [Fagbade and Omoway (2016)] studied numerically the model of natural convection boundary layer flow over a stretching porous surface kept as an isothermal in the presence of the effect of heat generation/absorption, chemical reaction, and thermal radiation. Fang et al. [Fang, An, Yu et al. (2020)] carried out the numerical study of the unsteady heat transfer phenomena about different complex geometries by using isogoemetric boundary element method. Hayat et al. [Hayat, Waqas, Shehzad et al. (2016)] predicted the problem of mixed convection flow about stagnation point flow taking Powell-Eyring fluid under the effect of heat generation/absorption, Newtonian heating, and thermal radiation. They predicted that a Prandtl number is increased temperature reduces and Nusslet number grows well. Kannan et al. [Kannan, Pullepu and Shehzad (2019)] considered the free convection boundary layer flow about a cone by considering the effect of thermal radiation, heat generation or absorption, magnetic field, and viscous dissipation. Authors solved the flow model by using the implicit finite difference method known as the Crank-Nicholson method and they concluded that fluid temperature is increased by increasing values of heat generation or absorption and increasing values of Pr lead to decrease in the temperature profile. Khan et al. [Khan, Sardar and Hashim (2018)] focused on convective heat transfer and fluid flow mechanism by considering Carreau fluid in the presence of the thermal radiation and heat generation/absorption effects. Effects of heat source and thermal radiation on heat transfer and fluid flow phenomenon with the inclusion of stagnation point are investigated by Khan et al. [Khan, Wqasa, Hayat et al. (2018)]. Matvienko et al. [Matvienko and Bailvlova (2015)] carried out the analysis on combustion of a swirling motion of air and methane mixture in the presence of paraxial porous insert. Mehmood et al. [Mehmood, Hussain and Sagheer (2016)] explored the transient mixed

convection flow past inclined stretching surface by considering the impacts of non-uniform heat absorption and generation. They found that increasing values mixed convection parameter and inclination angles lead to an increase in velocity of the fluid. On the other hand, like thermal conductivity parameter and heat source/sink increase results in intensification I temperature profile. Oni [Oni (2017)] investigated the mixed convection flow in vertical annulus geometry embedded in a porous medium and determined the analytical solution of the governing model. They have taken the effect of thermal radiation; heat source and porosity factor the medium on the considered physical properties. The study of fluid flow and heat transfer phenomenon on the continuously stretching surface with the effect of the non-uniform heat sink, heat source, and thermal radiation has been presented by Pal [Pal (2011)]. Their findings show that the increasing value of transient parameter results in a decrease in thermal and momentum boundary layer thickness. In addition, the velocity and temperature of the fluid flow domain fall down gradually owing to an increase in suction and injection parameter. Pal et al. [Pal and Mandal (2015)] examined the mixed convection flow at the stagnation point over the shrinking and stretching surface fixed in a porous medium by considering nanofluids in the presence of viscous dissipation and heat generation effects. It has been concluded from their findings that suction parameter causes to slow down the temperature and velocity profiles for the case of stretching surface and reverse behavior is seen for the case of the shrinking surface. Pop et al. [Pop, Grosan and Cornelia (2010)] studied numerically the phenomenon fully developed mixed convection flow through a vertical under the impact of heat which is generated by an exothermic chemical reaction. Shamshuddin et al. [Shamshuddin and Krishna (2019)] examined the unsteady flow problem of micropolar fluid along a vertical plate through porous medium with uniform plate velocity in the presence of heat generation and Joule heating effects. Umavathi et al. [Umavathi, Mallikarjun and Murthy (2013)] conducted the analysis on fully developed laminar combined forced and free convection accomplishing the effect of the magnetic field and heat generation or absorption. Yang et al. [Yang, Qian, Chu et al. (2017)] studied the rational bounds for error function and highlighted the approximated results. Yang et al. [Yang, Qian, Chu et al. (2018)] have given the idea of approximating error function.

From the above thorough research survey, we have come to the conclusion that no one has given the attention to the study of combined effects of nano particle material motion and heat generation /absorption for mixed convection flow along the surface of a sphere. We have modeled the problem of mixed convection flow around a sphere in the presence of nano particle material motion and heat generation/absorption effects. The flow model is made dimensionless and then finite difference scheme is used for integration of differential equations. The mathematical modeling and solution procedure of the problem is presented in the next sections as below.

2 Flow analysis

Consider, incompressible, viscous, steady, laminar, and two-dimensional fluid flows across the surface of a sphere at different circumferential positions. For the exhibition of the interesting study, the coordinate system is selected in such a way that the space coordinate $\bar{x}$ is chosen along the surface of a sphere and $\bar{y}$-axis is taken vertically to $\bar{x}$-axis. Here $\bar{x}/a$ and $\bar{r}(\bar{x})$ denote the angle subtended at the center of the sphere and radial

distance from the symmetric axis to the surface of a sphere with a designated as the radius of a sphere respectively. The temperature of the sphere surface is kept at T_w and mass concentration is taken C_w. The ambient temperature and mass concentration of the fluid are symbolized by T_∞ and C_∞ with the condition $T_w > T_\infty$ and $C_w > C_\infty$. The flow configuration and coordinate system are presented in Fig. 1. The governing continuity, momentum, energy, and mass equations along with subjected boundary conditions are given as below:

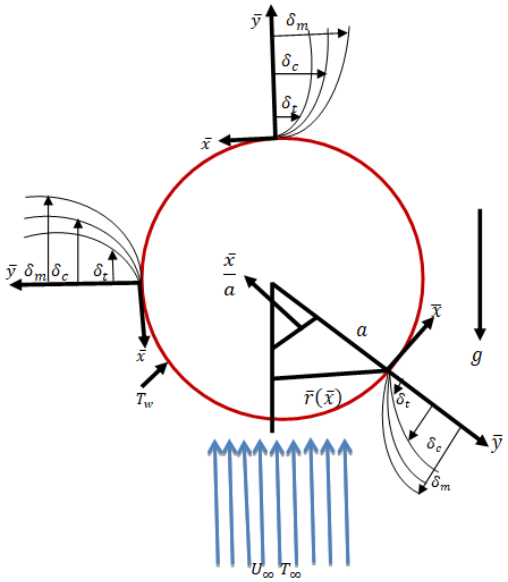

Figure 1: Coordinate system and flow configuration

$$\frac{\partial(\sin x\, u)}{\partial x} + \frac{\partial(\sin x\, v)}{\partial y} = 0, \tag{1}$$

$$u\frac{\partial u}{\partial x} + v\frac{\partial u}{\partial y} = \frac{\partial^2 u}{\partial y^2} + \lambda_t \theta sinx + \lambda_c \phi sinx, \tag{2}$$

$$u\frac{\partial \theta}{\partial x} + v\frac{\partial \theta}{\partial y} = \frac{1}{Pr}\frac{\partial^2 \theta}{\partial y^2} + \delta\theta\,, \tag{3}$$

$$u\frac{\partial \phi}{\partial x} + v\frac{\partial \phi}{\partial y} = \frac{1}{Sc}\frac{\partial^2 \phi}{\partial y^2} - \frac{\partial(v_t \phi)}{\partial y}. \tag{4}$$

Here are some notations used like mixed convection parameter $\lambda_t = Gr_t/Re^2$, modified mixed convection parameter $\lambda_c = Gr_c/Re^2$, Grashof number $Gr_t = g\,\beta_t(T - T_\infty)a^3/\nu^2$, modified Grashof number $Gr_c = g\,\beta_c(C - C_\infty)a^3/\nu^2$,Reynolds number $Re = U_\infty a/\nu$, Prandtl number, $Pr = \nu/\alpha$, heat generation absorption parameter $\delta = Q_o a/\rho\nu U_\infty$, and Schmidt number $Sc = \nu/D_m$. Here, we introduce thermophoretic or nano particle material velocity in Eq. (4), of the form given as below:

$$v_t = -\frac{k}{\theta + N_t}\frac{\partial \theta}{\partial y}\,,$$

Appropriate dimensionless forms of the boundary conditions are

$u = 0, v = 0,\ \theta = 1,\ \phi = 1$ at $y = 0,$

$u \to 1,\ \theta \to 0,\ \phi \to 0,$ as$y \to \infty.$ (5)

3 Solution methodology

Eqs. (1)-(5) are transformed into convenient form for integration by using the following the transformation variables

$u(x,y) = U(X,Y), v(x,y) = x^{-\frac{1}{2}}V(X,Y), Y = x^{-\frac{1}{2}}y, X = x, v_t(x,y) =$
$x^{-\frac{1}{2}}V_t(X,Y), \theta(x,y) = X^{-1}\theta(\mathrm{X},\mathrm{Y}), \phi(x,y) = X^{-1}\phi(\mathrm{X},\mathrm{Y}).$ (6)

By using the above primitive variable formulation given in Eq. (6) the governing conservation Eqs. (1)-(5) to obtain the following form:

$XU\,cosX + (X\frac{\partial U}{\partial X} - \frac{Y}{2}\frac{\partial U}{\partial Y} + \frac{\partial V}{\partial Y})sinX = 0,$ (7)

$XU\frac{\partial U}{\partial X} + \left(V - \frac{YU}{2}\right)\frac{\partial U}{\partial Y} = \frac{\partial^2 U}{\partial Y^2} + \lambda_t\theta\ \mathrm{sinX} + \lambda_c\phi\ \mathrm{sinX},$ (8)

$XU\frac{\partial \theta}{\partial X} + \left(V - \frac{YU}{2}\right)\frac{\partial \theta}{\partial Y} - U\theta = \frac{1}{Pr}\frac{\partial^2 \theta}{\partial Y^2} + X\delta\theta,$ (9)

$XU\frac{\partial \phi}{\partial X} + \left(V - \frac{YU}{2}\right)\frac{\partial \phi}{\partial Y} - U\phi = \frac{1}{Sc}\frac{\partial^2 \phi}{\partial Y^2} - \frac{\partial(V_t\phi)}{\partial Y},$ (10)

where $V_t = -\frac{k}{\theta + \mathrm{X}\,\mathrm{N_t}}\frac{\partial \theta}{\partial Y}.$

The primitive form of boundary conditions is

$U = 0, V = 0, \theta = 1, \phi = 1,$ at $Y = 0,$

$U \to 1, \theta \to 0, \phi \to 0,$ as $\mathrm{Y} \to \infty.$ (11)

3.1 Solution technique

The numerical solutions of the problem under consideration are obtained by using finite difference method. The Eqs. (7)-(10) along with boundary conditions Eq. (11) are transformed into difference form out of which we obtain system of algebraic equations. The central difference is employed to diffusion terms, and backward difference to convective terms. The general form of discretized equation is given in Eq. (12) as below

$A\psi_{i-1,j} + B\psi_{i,j} + C\psi_{i+1,j} = D,$ (12)

where A, B, C and D represent coefficient matrices of the general form of governing equations. The notation ψ denotes the variables $U, \theta,$ and ϕ. The block matrix Thomas algorithm is implemented for the numerical evaluation of the finite difference Eq. (12). The variables $U, \theta,$ and ϕ along with their derivatives are computed by using the Gaussian-elimination technique. The obtained numerical solutions are presented in graphical as well as in a tabular form. Software package Fortran Lahey-95 is used for the numerical solutions of the flow model and graphical software Tecplot 360 is used to display the obtained numerical results in graphical form.

3.2 Group of stream function formulation

Now we determine the similarity solutions of the Eqs. (1)-(4), so for this purpose we have to transform the dimensionless form of the partial differential Eqs. (1)-(4) into ordinary differential equations. For the transformation of the partial differential Eqs. (1)-(4) into ordinary differential equations, we use the following group of stream function formulation as

$$X = x, \eta = \frac{y}{X^{1/2}}, \psi(x,y) = X^{\frac{1}{2}} f(\eta), \theta(x,y) = \theta(\eta), \phi(x,y) = \phi(\eta). \tag{13}$$

where η is similarity variable, ψ is non-dimensional stream function usually taken as $ru = \partial(r\psi)/\partial y$ and $rv = -\partial(r\psi)/\partial x$, $\theta(\eta)$ is the dimensionless temperature profile and $\phi(\eta)$ is the dimensionless concentration profile. Using Eq. (13) the equation of continuity (1) is satisfied automatically, whereas Eqs. (2)-(4) reduce to the following similarity equations

$$f''' + \left(\frac{1}{2} + XcotX\right) ff'' + XsinX(\lambda_t \theta + \lambda_c \phi) = 0, \tag{14}$$

$$\frac{1}{Pr}\theta'' + \left(\frac{1}{2} + XcotX\right) f\theta' + X\delta\theta = 0, \tag{15}$$

$$\frac{1}{Sc}\phi'' + \left(\frac{1}{2} + XcotX\right) f\phi' + \frac{k}{Nt+\theta}\left(\theta'\phi' + \phi\theta'' - \frac{\phi\theta'^2}{Nt+\theta}\right) = 0. \tag{16}$$

where prime notation indicates the differentiation w. r. t η.

Associated boundary conditions are

$$f = 0, f' = 0,\ \theta = 1,\ \phi = 1 \text{ at } \eta = 0,$$
$$f' \to 1,\ \theta \to 0,\ \phi \to 0, \quad \text{as } \eta \to \infty. \tag{17}$$

The transformed thermophoretic or nano particle material velocity is given by

$$V_t = -\frac{k}{\theta + N_t}\theta'(0).$$

The transformed system of ordinary differential Eqs. (14)-(16) with boundary conditions (17) are solved by using built-in Numerical Solver BVP4C. BVP4C stands for boundary value problem fourth order scheme and it is built-in function for the numerical purpose of the boundary value problems. The similar solutions obtained by this scheme for the skin friction, the rate of heat transfer and the rate of mass transfer for different values of mixed convection parameter, λ_t, and modified mixed convection parameter, λ_c, taking the other pertinent parameters constant at position $X = \pi/2$ are shown in Tabs. 1-6. The comparison of the solution of the flow model for some physical quantities obtained by FDM and BVP4C is given in Tabs. 1-6, and is concluded that results obtained by both schemes are in good agreement which shows the validation of solutions obtained by FDM applied to the primitive form of the partial differential equations.

4 Results and discussion

The present study is carried out on the investigations of the mechanism of nano material motion and heat generation/absorption due to mixed convection flow. The influences of emerging physical dimensionless parameters involved the combined mechanism of the flow model is investigated. The behaviors of fluid velocity U, temperature field θ, and

mass concentration ϕ along with skin friction, heat transfer rate, and mass transfer rate for various values pertinent dimensionless numbers are displayed in graphically as well as tabular representation. The main focus is laid down on effect of the positive values of δ which is considered as heat generation and negative values of δ which is attributed as heat absorption with influence of thermophoresis on the said quantities. Figs. 2(a)-2(c) are concerned with the effect of various values of heat generation parameter δ when the other material parameters are taken constant on main physical properties such as velocity profile, temperature profile, and mass concentration. It has been extracted from the graphical findings that increasing values of heat generation parameter cause the augmentation in velocity and temperature of the fluid flow domain. It is interesting to note that temperature distribution intensifies at position $X = \pi, \pi/4$ and reduces at $X = \pi/6$, and $\pi/2$, but on the other hand, the mass concentration decreases at location $X = \pi, \pi/4$ and increases at position $X = \pi/6\ \ \pi/2$. It is inevitable to point out that maximum magnitude for fluid velocity; fluid temperature and mass concentration are secured at positions $X = \pi/2, X = \pi,$ and $X = \pi$ respectively. Figs. 3(a)-3(c) show the behaviors of the same properties mentioned earlier in Figs. 2(a)-2(c) corresponding to various values of the heat absorption parameter. Graphical representation demonstrates that velocity and the temperature profiles are maximized at position $X = \pi/4$, but the mass concentration is minimized at the same position with same parametric conditions as heat absorption parameter is changed from $\delta = -0.1$ to $\delta = -0.3$. At location $X = \pi/2$, the velocity distribution decreases but mass concentration increases and no change is seen in temperature profile. Figs. 4(a)-4(c) present the variations in velocity field, the temperature profile, and the mass concentration for various values of mixed convection parameter and taking heat generation parameter $\delta = 0.3$. It is concluded from these graphs that velocity distribution increases at locations $X = \pi/6, \pi$ and decreases at points $X = \pi/4, \pi/2$ corresponding to increasing magnitudes of λ_t. It is seen that temperature profile goes down at all the assumed positions across the sphere's surface. It is deliberately observed that mass concentration gets reduced at point $X = \pi/6, \pi$ and curves march up at locations $X = \pi/4, \pi/2$. It is worth mentioning to note that velocity, temperature, and mass profiles attain the largest magnitudes at circumferential locations $X = \pi/2, \pi$ and π respectively. Figs. 5(a)-5(c) reveal the trends of considered properties for the case of the heat absorption parameter $\delta = -0.3$ for the similar other parametric conditions assumed in Figs. 4(a)-4(c). These sketches illuminate that the velocity field increases at all the positions but the reverse trend is viewed at point $X = \pi/2$. The pattern in Fig. 2(b) shows that temperature profile increases at $= \pi/6,\ \pi/4$ no change is recorded at $X = \frac{\pi}{2}, \pi$. The mass concentration pattern in Fig. 5(c) shows that it slows down at $= \pi/6, \pi/4$, and π but reverse attitude at observed at $X = \pi/2$. Figs. 6(a)-6(c) illustrate the effect of thermophoresis parameter N_t by taking it various values and heat generation parameter $\delta = 0.3$ when other dimensionless numbers are held fixed on the chief physical properties mentioned earlier. Figs. 6(a)-6(c) show that velocity and temperature fields increase at $X = \pi/6,\ \pi/4$ but decrease at $X = \pi/2$. No change is seen at $X = \pi$. From Fig. 6(c) we can conclude that mass concentration decreases at location $X = \pi/6, \pi/4$ and increases $X = \pi/2$. It is significant to demonstrate that

maximum magnitudes for velocity field, temperature field and mass concentration are obtained at $X = \pi/4, \pi$ and π respectively.

Figs. 7(a)-7(c) show the variations in the same considered physical properties with same parametric conditions already mentioned in Figs. 6(a)-6(c) with the inclusion of heat absorption parameter effects. For the case of heat absorption effects velocity profile is augmented at circumferential position $X = \pi/4, \pi/2,$ but reduces at $X = \pi/6$. Fig. 7(b) displays that temperature profile rises up drastically at position $X = \pi/2$ for increasing values of N_t but no variations are observed at the considered remaining positions. Similar behavior is observed in mass concentration that is it decreases at $X = \pi/2$ but no variations are seen at other locations. The effect of several values of nano particle material coefficient k and positive values of δ that is heat generation effect and negative values of δ that is heat absorption effect on main physical properties named earlier in the previous discussion are presented in Figs. 8(a)-8(c) and 9(a)-9(c). Graphical results in Figs. 8(a)-8(b) indicate that velocity and temperature fields are augmented at points $X = \pi/6, \pi/4$ but reduced at $X = \pi/2$. Fig. 8(c) shows mass concentration reduces at positions $X = \pi/6, \pi/4$ and intensified at $X = \pi/2$. The physical behavior of the velocity profile, temperature profile and mass concentration under the influence of heat absorption parameter for various values of the nano particle material coefficient are presented in Figs. 9(a)-9(c). Graphs 9(a)-9(b) are conveying that velocity field is enhanced at position $X = \pi/4$ but decreases at $X = \pi/2$ and no variations are located at $X = \pi/2$. Fig. 9(b) depicts that no changes are observed at all taken positions. Graphs plotted in Fig. 9(c) shows that mass concentration reduces at positions $X = \pi/4,$ with modifications observed at other positions $X = \pi/6, \pi$. It is to mark that at position $X = \pi/2$ mass concentration is increased. In addition, it is extracted from these graphical results that maximum magnitudes for velocity profile, temperature profile, and mass concentration are obtained at $X = \pi/2, \pi/2$ and $X = \pi$ respectively. Tabs. 1-6 are presenting the numerical results of the skin friction, the rate of heat transfer, and the rate of mass transfer obtained by finite difference method and built-in Numerical Solver BVP4C for different values of mixed convection parameter λ_t and modified mixed convection parameter λ_c by keeping other parametric condition constant at location $\pi/2$. Our numerical solutions obtained by FDM are validated by built-in Numerical Solver BVP4C at leading edge. We can see that the results obtained by both schemes are showing good agreement.

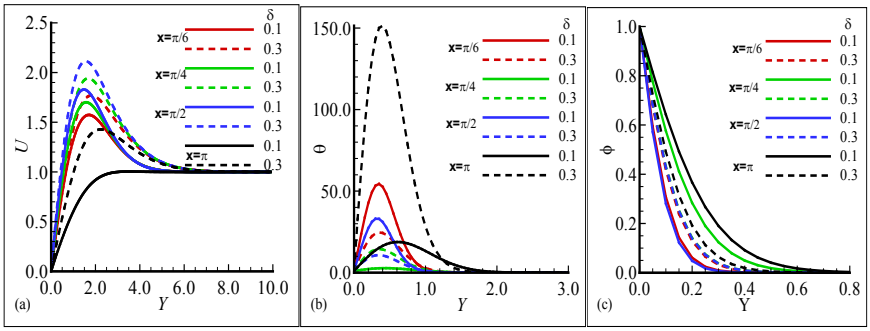

Figure 2: Plots of (a) U (b) θ and (c) ϕ for $\delta = 0.1, 0.3$ when $\lambda_t = 1.1, \lambda_c = 0.5, Sc = 0.5, k = 0.1,$ Pr=7.0 and $N_t = 0.4$

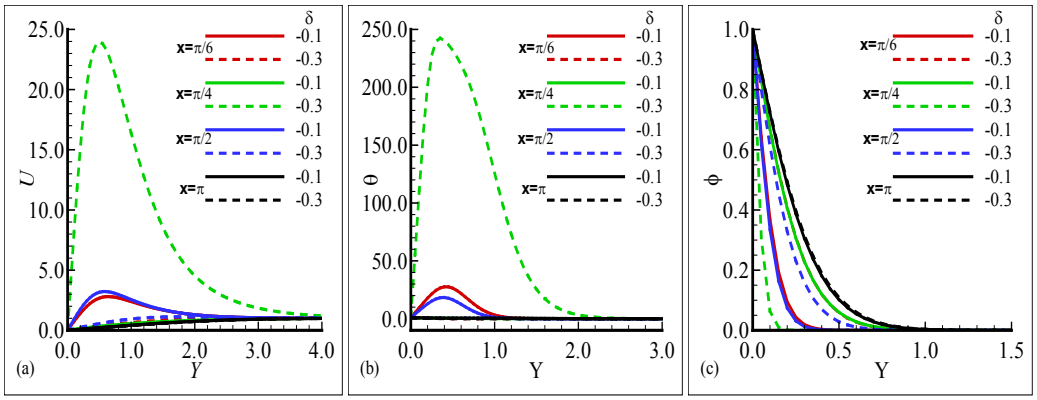

Figure 3: Plots of (a) U (b) θ and (c) ϕ for $\delta = -0.1, -0.3$ when $\lambda_t = 1.1, \lambda_c = 0.5, , Sc = 0.5, k = 0.1$, Pr=7.0 and $N_t = 0.4$

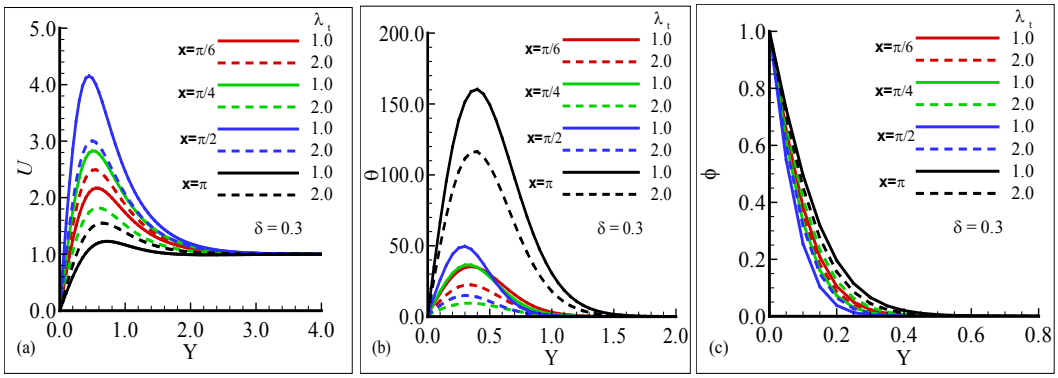

Figure 4: Plots of (a) U (b) θ and (c) ϕ for $\lambda_t = 1.0, 2.0$ when $\delta = 0.3, \lambda_c = 0.5, Sc = 0.5, k = 0.1$, Pr=7.0 and$N_t = 0.4$

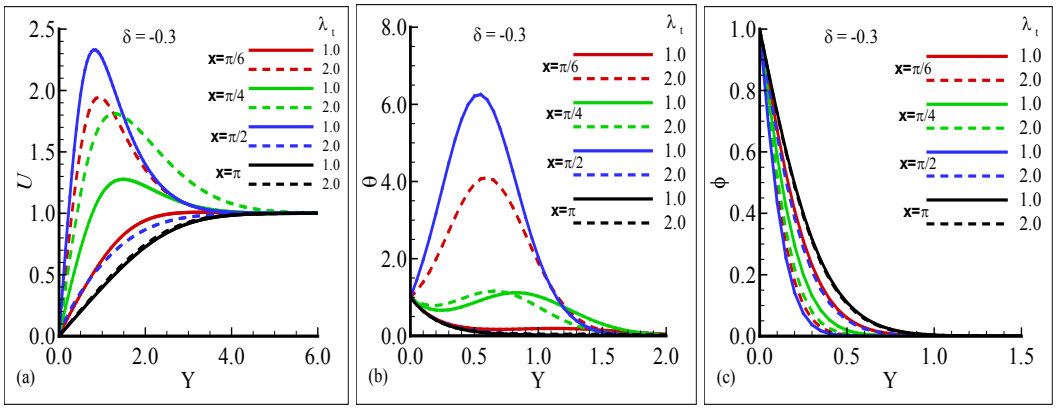

Figure 5: Plots of (a) U (b) θ and (c) ϕ for $\lambda_t = 1.0, 2.0$ when $\delta = -0.3, \lambda_c = 0.5, , Sc = 0.5, k = 0.1$, Pr=7.0 and $N_t = 0.4$

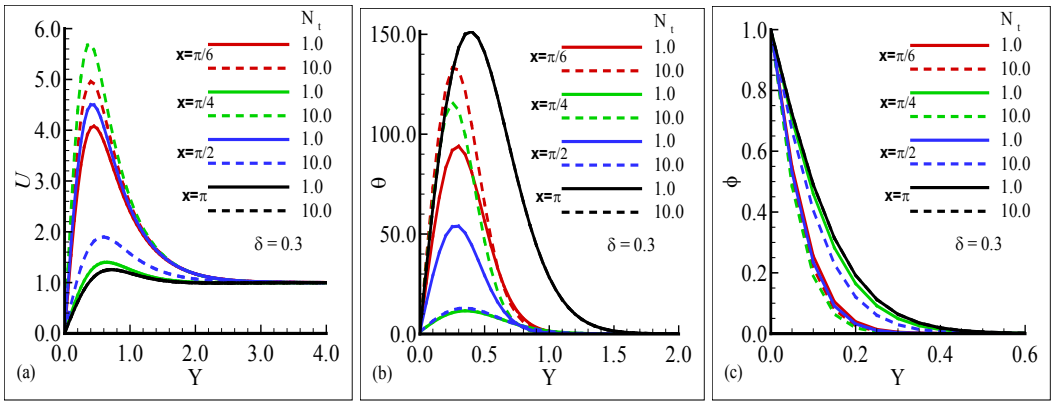

Figure 6: Plots of (a) U (b) θ and (c) ϕ for $N_t = 1.0, 10.0$ when $\delta = 0.3, \lambda_c = 0.5$, $\lambda_t = 1.1, k = 0.1$, Pr=7.0 and $Sc = 0.5$

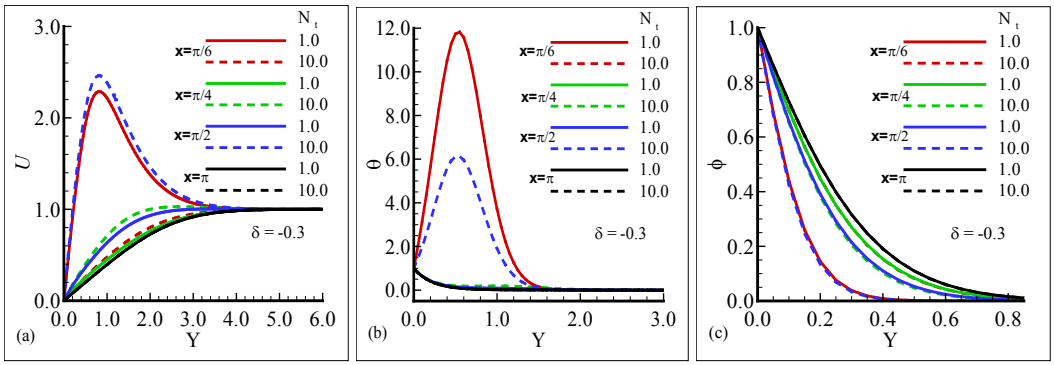

Figure 7: Plots of (a) U (b) θ and (c) ϕ for $N_t = 1.0, 10.0$ when $\delta = -0.3, \lambda_c = 0.5$, $\lambda_t = 1.1, k = 0.1$, Pr =7.0 and $Sc = 0.5$

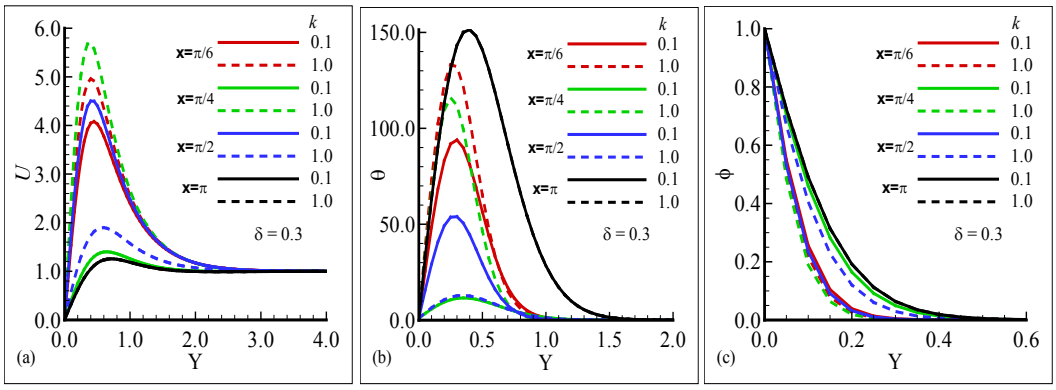

Figure 8: Plots of (a) U (b) θ and (c) ϕ for $k = 0.1, 1.0$ when $\delta = 0.3, N_t = 0.4, Pr = 7.0$, $\lambda_t = 1.1, \lambda_c = 0.5$, Pr=7.0 and $Sc = 0.5$

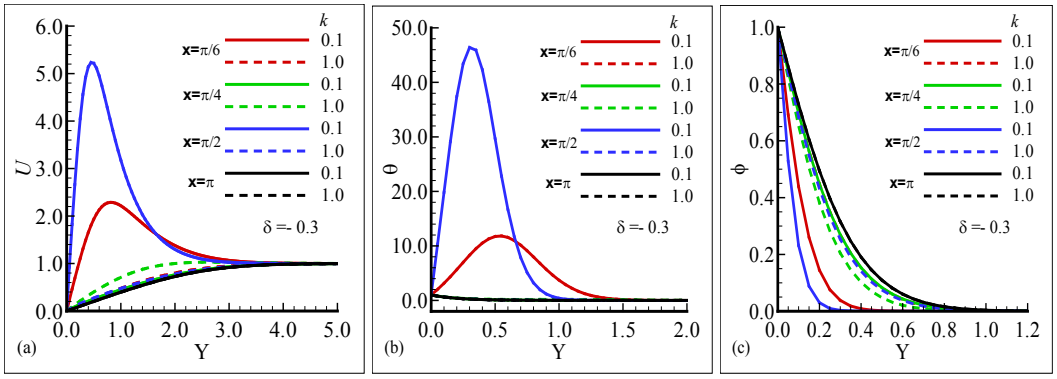

Figure 9: Plots of (a) U (b) θ and (c) ϕ for $k = 0.1, 1.0$ when $\delta = -0.3, N_t = 0.4, Pr = 7.0$, $\lambda_t = 1.1, \lambda_c = 0.5$, Pr=7.0 and $Sc = 0.5$

Table 1: Numerical results for the skin friction for different values of mixed convection parameter, λ_t, obtained by FDM and BVP4C when $X = \frac{\pi}{2}, \lambda_c = 10.0$, Pr = 0.71, $N_t = 1.0, k = 1.0$, Sc=10.0, and $\delta = 0.3$

λ_t	$\left(\frac{\partial U}{\partial Y}\right)_{Y=0}$	
	FDM	BVP4C
1.0	7.56603	7.59212
3.0	8.52699	8.56687
5.0	9.52050	9.53140
7.0	10.48610	10.48638
9.0	11.43404	11.43232

Table 2: Numerical results for the rate of heat transfer for different values of mixed convection parameter, λ_t, obtained by FDM and BVP4C when $X = \frac{\pi}{2}, \lambda_c = 10.0$, Pr = 0.71, $N_t = 1.0, k = 1.0$, Sc=10.0, and $\delta = 0.3$

λ_t	$\left(\frac{\partial \theta}{\partial Y}\right)_{Y=0}$	
	FDM	BVP4C
1.0	0.90655	0.90948
3.0	0.91337	0.91670
5.0	0.92108	0.92378
7.0	0.93650	0.93074
9.0	0.93629	0.93757

Table 3: Numerical results for the rate of mass transfer for different values of mixed convection parameter, λ_t, obtained by FDM and BVP4C when $X = \frac{\pi}{2}, \lambda_c = 10.0$, Pr = 0.71, $N_t = 1.0, k = 1.0$, Sc=10.0, and $\delta = 0.3$

λ_t	$\left(\frac{\partial \phi}{\partial Y}\right)_{Y=0}$	
	FDM	BVP4C
1.0	0.53026	0.53068
3.0	0.54059	0.54094
5.0	0.55101	0.55167
7.0	0.56113	0.56288
9.0	0.57354	0.57456

Table 4: Numerical results for the skin friction for different values of modified mixed convection parameter, λ_c, obtained by FDM and BVP4C when $X = \frac{\pi}{2}, \lambda_t = 10.0$, Pr = 0.71, $N_t = 1.0, k = 1.0$, Sc=10.0, and $\delta = 0.3$

λ_c	$\left(\frac{\partial U}{\partial Y}\right)_{Y=0}$	
	FDM	BVP4C
1.0	6.74929	6.90665
3.0	8.03446	8.07725
5.0	9.18293	9.21314
7.0	10.26673	10.31417
9.0	11.35865	11.38105

Table 5: Numerical results for the rate of heat transfer for different values of modified mixed convection parameter, λ_c, obtained by FDM and BVP4C when $X = \frac{\pi}{2}, \lambda_t = 10.0$, Pr = 0.71, $N_t = 1.0, k = 1.0$, Sc=10.0, and $\delta = 0.3$

λ_c	$\left(\frac{\partial \theta}{\partial Y}\right)_{Y=0}$	
	FDM	BVP4C
1.0	0.90951	0.90128
3.0	0.91016	0.91094
5.0	0.92009	0.92011
7.0	0.92717	0.92879
9.0	0.93385	0.93701

Table 6: Numerical results for the rate of mass transfer for different values of modified mixed convection parameter, λ_c, obtained by FDM and BVP4C when $X = \frac{\pi}{2}, \lambda_t = 10.0$, Pr = 0.71, $N_t = 1.0, k = 1.0$, Sc=10.0, and $\delta = 0.3$

λ_c	$\left(\frac{\partial \phi}{\partial Y}\right)_{Y=0}$	
	FDM	BVP4C
1.0	0.51062	0.51990
3.0	0.53124	0.53282
5.0	0.54468	0.54609
7.0	0.55680	0.55972
9.0	0.57207	0.57358

5 Concluding Remarks

The current numerical results are computed for the model of viscous, incompressible, steady, and two-dimensional flow under the impacts of thermophoretic or nano particle material transportation and heat generation/absorption by employing finite difference scheme around the surface of considered geometry at its different locations. After a deliberate investigation of the impact of pertinent parameters on the encountered chief physical quantities, the following key features are extracted from our current research study. It has been extracted from the graphical findings that increasing values of heat generation parameter causes the augmentation in velocity of the fluid flow domain. It is interesting to note that temperature distribution intensifies at position $X = \pi, \pi/4$ and reduces at $X = \pi/6$, $\pi/2$ but on the other hand, the mass concentration decreases at location $X = \pi/4, \pi$ and increases at position $X = \pi/6, \pi/2$. Numerical results demonstrate that velocity and the temperature profiles are maximized at position $X = \pi/4$ but the mass concentration is minimized at the same position with same parametric conditions as heat absorption parameter is changed from $\delta = -0.1$ to $\delta = -0.3$. At location $X = \pi/2$, the velocity distribution decreases but mass concentration increases and no change is seen in temperature profile. It is concluded from these graphs that velocity distribution increases at locations $X = \pi/6, \pi$ and decreases at points $X = \pi/4, \pi/2$ corresponding to increasing magnitudes of λ_t. It is seen that temperature profile goes down at all the assumed positions across the sphere surface. It is deliberately observed that mass concentration gets reduced at point $X = \pi/6, \pi$ and curves march up at locations $X = \pi/4, \pi/2$. For the case heat absorption effects velocity profile is augmented at circumferential positions $X = \pi/6, \pi/4, \pi/2$ and π but reduces at $X = , \pi/2$. Numerical solutions displays that temperature profile rises up at position $X =, \pi/2$ for increasing values of N_t but no variations are observed at the considered remaining positions. Similar behavior is observed in mass concentration. The numerical results for the skin friction, the rate of heat transfer, and the rate of mass transfer obtained by FDM are validated by built-in Numerical Solver BVP4C at the leading edge and the comparison of numerical solutions determined by both schemes is presented in Tabs. 1-6. It is concluded that numerical findings of the physical properties by both methods show the good agreement between them. From numerical results presented in the present work, it is

noticed that as the values of δ is increased from $\delta = 0.1$ to $\delta = 0.3$ the skin friction and heat transfer rate increase but mass transfer rate decreases at the same parametric conditions.

Acknowledgment: The authors would like to acknowledge Natural Science Foundation of China (Grant Nos. 61673169, 11701176, 11626101, 11601485).

Funding Statement: This research was funded by the Natural Science Foundation of China (Grant Nos. 61673169, 11701176, 11626101, 11601485).

Conflicts of Interest: The authors declare no conflicts of interest.

References

Abbas, A.; Ashraf, M. (2020): Combined effects of variable viscosity and thermophoretic transportation on mixed convection flow around the surface of a sphere. *Thermal Science*.

Ashraf, M., Khan, A.; Gorla, R. S. R. (2019); Natural convection boundary layer flow of nanofluids around different stations of the sphere and into the plume above the sphere. *Heat Transfer-Asian Research*, vol. 48, no. 3, pp. 1127-1148.

Ashraf, M.; Chamkha, A. J.; Iqbal, S.; Ahmad, M. (2016): Effects of temperature-dependent viscosity and thermal conductivity on mixed convection flow along a magnetized vertical surface. *International Journal of Numerical Methods for Heat and Fluid Flow*, vol. 26, no. 5, pp. 1580-1592.

Ashraf, M.; Fatima, A. (2018): Numerical simulation of the effect of transient shear stress and the rate of heat transfer around different positions of sphere in the presence of viscous dissipation. *Journal of Heat Transfer*, vol. 140, no. 6, pp. 701-7012.

Ashraf, M.; Fatima, A.; Gorla, R. S. R. (2017): Periodic momentum and thermal boundary layer mixed convection flow around the surface of a sphere in the presence of viscous dissipation. *Canadian Journal of Physics*, vol. 95, no. 10, pp. 976-986.

Ashraf, M.; Ullah, Z. (2020): Effects of variable density on oscillatory flow around a non-conducting horizontal circular cylinder. *American Institute of Physics (AIP) Advances*, vol. 10.

Fagbade, A. I.; Omowaye, A. J. (2016): Influence of thermal radiation on free convective heat and mass transfer past an isothermal vertical oscillating porous plate in the presence of chemical reaction and heat generation-absorption. *Boundary Value Problems*, vol. 97, no. 1, pp. 1-18.

Fang, W.; An, Z.; Yu, T.; Bui, T. Q. (2020): Analysis of the unsteady heat transfer problems with complex geometries using isogeometric boundary element method. *Computers, Materials & Continua*, vol. 62, no. 2, pp. 929-962.

Hayat, T.; Waqas, M.; Shehzad, S. A.; Alsaedi, A. (2016): Mixed convection stagnation-point flow of Powell-Eyring fluid with Newtonian heating, thermal radiation, and heat generation/absorption. *Journal of Aerospace Engineering*, vol. 30, no. 1, 04016077.

Kannan, R. M.; Pullepu, B.; Shehzad, S. A. (2019): Numerical solutions of dissipative natural convective flow from a vertical cone with heat absorption, generation, MHD and

radiated surface heat flux. *International Journal of Applied and Computational Mathematics*, vol. 5, no. 1, pp. 24.

Khan, M.; Sardar, H.; Hashim (2018): Heat generation/absorption and thermal radiation impacts on three-dimensional flow of Carreau fluid with convective heat transfer. *Journal of Molecular Liquids*, vol. 272, pp. 474-480.

Khan. M. I.; Wqasa, M.; Hayat, T.; Imran, M.; Alsaedi, A. (2018): Melting heat transfer in stagnation point of Carreau fluid with non-linear thermal radiation and heat source. *Journal of the Brazilian Society of Mechanical Sciences and Engineering*, vol. 40, no. 5, pp. 270.

Matvienko, O. V.; Baigulova, A. I. (2015): Study of the influence of a paraxial porous insert on combustion of a swirling flow of a mixture of methane and air. *Russian Physics Journal*, vol. 58, no. 3, pp. 304-310.

Mehmood, K.; Hussain, S.; Sagheer, M. (2016): Mixed convection flow with non-uniform heat source/sink in a doubly stratified magnetonanofluid. *American Institute of Physics (AIP) Advances*, vol. 6, no. 6, 065126.

Oni, M. O. (2017): Combined effect of heat source, porosity and thermal radiation on mixed convection flow in a vertical annulus: an exact solution. *Engineering Science and Technology, An International Journal*, vol. 20, no. 2, pp. 518-527.

Pal, D. (2011): Combined effects of non-uniform heat source/sink and thermal radiation on heat transfer over an unsteady stretching permeable surface. *Communications in Nonlinear Science and Numerical Simulation*, vol. 16, no. 4, pp. 1890-1904.

Pal, D.; Mandal, G. (2015): Mixed convection-radiation on stagnation-point flow of nanofluids over a stretching/shrinking sheet in a porous medium with heat generation and viscous dissipation. *Journal of Petroleum Science and Engineering*, vol. 126, pp. 16-25.

Pop, I.; Grosan, T.; Cornelia, R. (2010): Effect of heat generated by an exothermic reaction on the fully developed mixed convection flow in a vertical channel. *Communications in Nonlinear Science and Numerical Simulation*, vol. 15, no. 3, pp. 471-474.

Shamshuddin, M. D.; Krishna, C. B. (2019): Heat absorption and Joule heating effects on transient free convective reactive micropolar fluid flow past a vertical porous plate. *Fluid dynamics and Material Research*, vol. 15, no. 3, pp. 207-231.

Umavathi, J. C.; Mallikarjun, B. P.; Murthy, S. N. (2013): On laminar magnetoconvection flow in a vertical channel in the presence of heat generation and heat absorption. *Journal of Heat Transfer*, vol. 135, no. 4, 042503.

Yang, Z. H.; Qian, W. M.; Chu, Y. M.; Zhang, W. (2017): On rational bounds for gamma function. *Journal of Inequalities and Applications*, no. 1, pp. 210.

Yang, Z. H.; Qian, W. M.; Chu, Y. M.; Zhang, W. (2018): On approximating the error function. *Mathematical Inequalities and Applications*, vol. 21, no. 2, pp. 469-479.